

Impact of different parameterization schemes on simulation of mesoscale convective system over south-east India

A. Madhulatha¹ · M. Rajeevan²

Received: 15 November 2016 / Accepted: 18 January 2017 / Published online: 30 January 2017
© Springer-Verlag Wien 2017

Abstract Main objective of the present paper is to examine the role of various parameterization schemes in simulating the evolution of mesoscale convective system (MCS) occurred over south-east India. Using the Weather Research and Forecasting (WRF) model, numerical experiments are conducted by considering various planetary boundary layer, microphysics, and cumulus parameterization schemes. Performances of different schemes are evaluated by examining boundary layer, reflectivity, and precipitation features of MCS using ground-based and satellite observations. Among various physical parameterization schemes, Mellor–Yamada–Janjic (MYJ) boundary layer scheme is able to produce deep boundary layer height by simulating warm temperatures necessary for storm initiation; Thompson (THM) microphysics scheme is capable to simulate the reflectivity by reasonable distribution of different hydrometeors during various stages of system; Betts–Miller–Janjic (BMJ) cumulus scheme is able to capture the precipitation by proper representation of convective instability associated with MCS. Present analysis suggests that MYJ, a local turbulent kinetic energy boundary layer scheme, which accounts strong vertical mixing; THM, a six-class hybrid moment microphysics scheme, which considers number concentration along with mixing ratio of rain hydrometeors; and BMJ, a closure

cumulus scheme, which adjusts thermodynamic profiles based on climatological profiles might have contributed for better performance of respective model simulations. Numerical simulation carried out using the above combination of schemes is able to capture storm initiation, propagation, surface variations, thermodynamic structure, and precipitation features reasonably well. This study clearly demonstrates that the simulation of MCS characteristics is highly sensitive to the choice of parameterization schemes.

1 Introduction

Representation of physical processes related to boundary layer, cloud microphysics, and convection plays an important role in simulation of mesoscale convective systems (Cintineo et al. 2014). Proper description of these processes is one of the most challenging tasks in mesoscale numerical simulation and prediction. In general, Numerical weather prediction (NWP) models use parameterization schemes to characterize the effect of these subgrid-scale physical processes using resolvable scale fields. Therefore, proper choice of different parameterization schemes plays crucial role in simulation of severe convective systems.

Vertical transfer of heat, moisture, and momentum between surface and atmosphere is essential to understand the evolution of planetary boundary layer (PBL). Accurate representation of PBL and atmospheric stability in severe weather environment is dependent on PBL parameterization schemes. Mixing associated with turbulent eddies results in exchange of fluxes and influence the lower thermodynamic and kinematic structure, and impacts the cloud development (Cohen et al. 2015). Different cloud

Responsible Editor: S. Hong.

✉ A. Madhulatha
madhulatha11@gmail.com

¹ National Atmospheric Research Laboratory, Department of Space, Gadanki 517112, India

² Ministry of Earth Sciences, New Delhi 110003, India

microphysical processes are important to explain the cloud life cycle and precipitation efficiency. Cloud microphysics parameterization schemes accounts formation of different types of hydrometeors and complex interactions between them. These processes directly impact buoyancy and resulting convective fluxes through condensate loading and latent heating/cooling due to phase changes and affect the storm-scale dynamics and precipitation accumulation (Morrison et al. 2009). To explain the cumulus convection, latent heat release, and redistribution of heat, moisture and momentum associated with the mass transport of cumulus updrafts and downdrafts are important. Accurate representation of convective initiation, timing, and location in a mesoscale model is dependent on cumulus parameterization schemes. These schemes strongly influence the simulated rainfall patterns by accounting the collective effects of ensembles of discrete convective bubbles or plumes (Arakawa and Schubert 1974).

From the aforementioned synthesis, it is well demonstrated that the choice of physical parameterization schemes has important effects on the simulation of severe convective systems. Numerous sensitivity studies for one or more physics options of WRF model have been undertaken in different parts of world (Jankov et al. 2005; Krieger et al. 2009; Ruiz et al. 2010; Flaounas et al. 2011; Ferreira et al. 2014). Role of different PBL schemes on simulating turbulent vertical fluxes in the boundary layer and convective initiation of severe convective systems is reported by Wisse and Arellano (2004), Fabry (2006), Pliem (2007), Shin and Hong (2011) and Coniglio et al. (2013). Effect of different microphysical schemes in distribution of different hydrometeors and simulation of storm-scale dynamics is evaluated by Otkin et al. (2006), Hong et al. (2009), Morrison and Milbrandt (2011), and Weverberg et al. (2012). Model sensitivity to convective parameterization schemes in representing the mass transport and simulation of deep convection has been explored in many studies (Wang and Seaman 1996; Dudhia et al. 2002; Melissa and Mullen 2005; Gilland and Rowe 2007; Pennely et al. 2014).

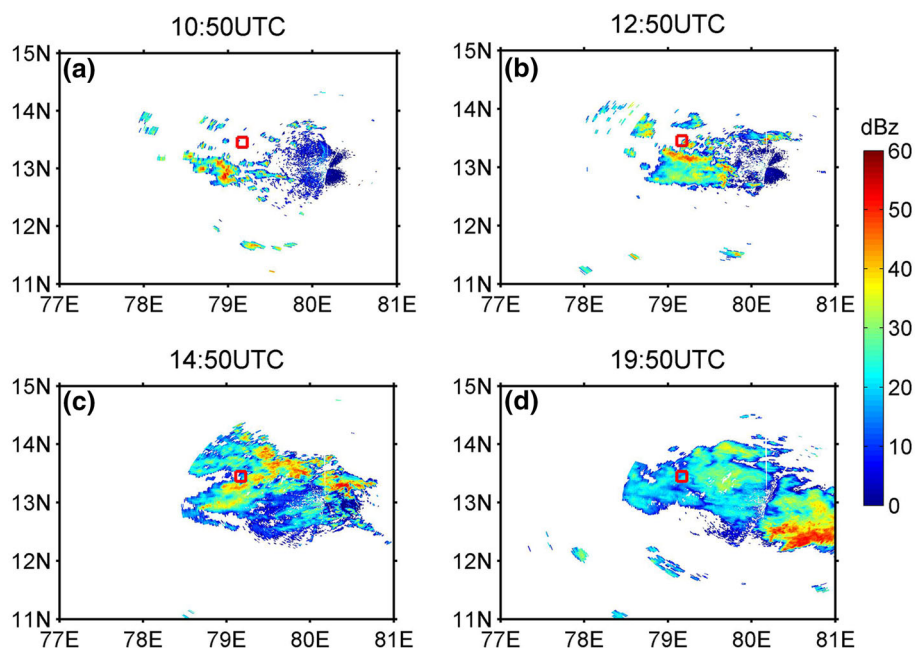
Over Indian region, sensitivity to different parameterization schemes on simulation of severe weather events has been addressed by many researchers which mainly focused on events like tropical cyclone (Rao and Prasad 2007; Pattanayak and Mohanty, 2008; Mukhopadhyay et al. 2011), heavy precipitation (Rama Rao et al. 2007; Vaidya and Kulkarni 2007; Deb et al. 2010; Kumar et al. 2010), thunderstorm (Chatterjee et al. 2008), and also model performance to different physics schemes over subtropical region (Manju mohan and Bhati 2011). The microphysical structure associated with tropical cloud clusters using MM5 is reported by Abhilash et al. 2008. In a study by Litta and Mohanty 2008, potential of high-resolution models in

providing unique and valuable information for severe thunderstorm forecasts is demonstrated. Sensitivity of cloud microphysics in predicting the structure of severe convective storms over south-east India has been addressed by Rajeevan et al. 2010. They emphasize the need to study the role of cumulus schemes along with microphysics on simulation of severe convective events. Recent study by Fadnavis et al. 2014 compared the performance of different cumulus schemes in simulating heavy rain associated with the thunderstorm. Effect of boundary layer schemes in simulating the atmospheric instability in prestorm environment is investigated by Madala et al. 2016. Although most of above-mentioned studies have examined the roles of different physical schemes in the numerical simulation of severe convective events, the influence of physical schemes on simulation of storm development is less understood. In addition, the impact of different PBL, microphysics, and cumulus schemes on the simulation of severe convective events over south-east India have received very little attention. No systematic efforts have been made to examine the sensitivity of boundary layer, microphysics, and cumulus schemes all together. Therefore, the main objective of this study is twofold: (1) to investigate the general impact of various physical schemes on simulation of severe convective events over south-east India; (2) to explore the possible reasons for differences between simulations. To investigate these issues, MCS passed over Gadanki (13.5°N, 79.2°E) located at south-east India is considered for simulation. Various numerical experiments are carried out using WRF model to examine the skill of MCS simulation to different physical schemes. Possible reasons for the performance difference in various physical schemes are investigated by comparing with available observations. The layout of this paper is as follows; in Sect. 2, data and methodology are discussed; brief description of MCS along with synoptic features responsible for the formation of MCS is explained. Description of model, sensitivity schemes, and experimental setup are described in Sect. 3. Sensitivity of model simulations to different boundary layer, microphysics, and cumulus parameterization schemes is discussed in Sect. 4. Model simulation carried out using final combination of physical schemes is assessed by utilizing the available observations in Sect. 5. Conclusions are drawn in Sect. 6.

2 Data and methodology

MCS developed over south-east India on 27th July 2011 is identified using reflectivity observations from Doppler Weather Radar (DWR), India Meteorological Department, Chennai (13.1°N, 80°E). Associated with the passage of this MCS, a convective system has swept over Gadanki

Fig. 1 Spatial map of DWR reflectivity (dBz) at **a** 10:50 UTC, **b** 12:50 UTC, **c** 14:50 UTC, and **d** 19:50 UTC on 27th July 2011. Open red square in the figure represents the study region ((13.5°N/79.2°E) Gadanki)



(study region), a semi arid region over south-east India. It is a super observational site with variety of meteorological instruments and is about 120 km to the northwest of Chennai. Numerical experiments are performed using high-resolution nested WRF model by employing different physical parameterization schemes. System evolution is studied using DWR observations and spatial variability of model simulated surface parameters is examined using Indian Space Research Organization (ISRO) Automatic Weather Stations (AWS) network (data available at <http://www.mosdac.gov.in>). Model simulated accumulated precipitation is validated using Global satellite Mapping of Precipitation (GsMAP) observations available at hourly intervals with 0.1° horizontal resolution (Okamoto et al. 2005). Variations in surface features, vertical stability, and thermodynamic structure of atmosphere during MCS passage over Gadanki are studied using Automatic Weather Station (AWS), GPS radiosonde, and Microwave Radiometer (MWR) observations.

2.1 Mesoscale convective event: 27th July 2011

Spatial maps of DWR reflectivity are shown in Fig. 1, which explains the initiation, development, and decay of MCS. Around 10:50 UTC (Fig. 1a), MCS is developed southwest to the study region, associated with this a convective system passed over Gadanki around 12:50 UTC with reflectivity around 40 dBz (Fig. 1b). Later, a second convective system is observed around 14:50 UTC (Fig. 1c) with high reflectivity values which has further propagated towards east of the study region around 19:50 UTC (Fig. 1d). To understand the temporal evolution and vertical distribution of convective system over Gadanki, time-height cross section of

reflectivity is analyzed (Fig. 2). Strong convective activity with reflectivity greater than 40 dBz is observed. Double cell structure is clearly visible with intense cell around 13:30 UTC with reflectivity ~ 35 dBz and another cell around 15:30 UTC with reflectivity >40 dBz. Vertical extent of first convective cell is reaching up to 6 km and the second convective cell has a vertical extent of 7 km. The system has sustained for 7–8 h over the study region (Fig. 2).

Synoptic conditions during pre-environment of the storm are examined using MERRA (Modern Era Retrospective Analysis for Research and Applications) reanalysis data at 12:00 UTC of 27th July 2011. From Fig. 3a, it is noticed that a north–south trough is present over south-eastern part of India which resulted in low-level cyclonic vorticity. Strong westerly north westerlies are seen along and adjoining the study region associated with the monsoon circulation. Large amount of relative humidity ($>80\%$) is observed over west of the study region (Fig. 3b). Latitude-height cross section fixed at Gadanki longitude

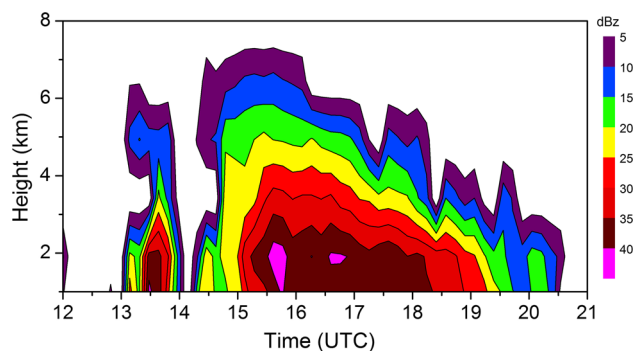


Fig. 2 Time–height cross section of DWR reflectivity (dBz) over Gadanki during 27th July 2011

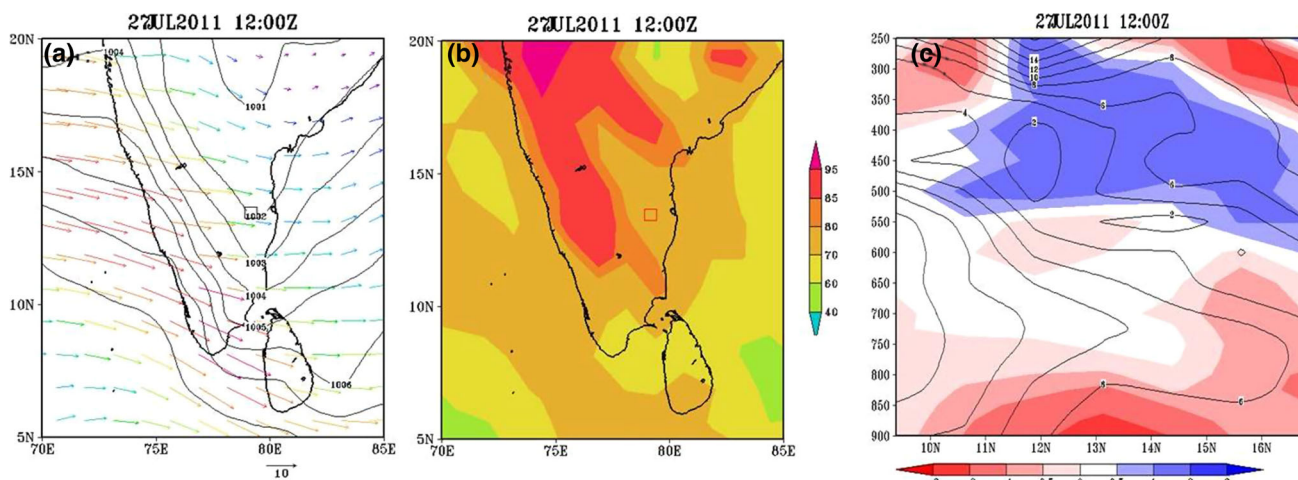


Fig. 3 Spatial maps from MERRA at 12:00 UTC of 27th July 2011 of **a** mean sea level pressure (MSLP in hPa) and wind vectors (m/s) at 850 hPa, **b** relative humidity (%) at 850 hPa, and **c** latitude-height

cross section (at Gadanki longitude 79.2°E) of horizontal divergence (10^5 s^{-1} , shaded)

(79.2°E) shows strong low-level convergence and upper level divergence over the study region (Fig. 3c). Analysis suggests that large-scale monsoon synoptic forcing has created the favourable environment for the genesis of convective storm southwest of Gadanki on 27th July 2011.

3 WRF model description

High-resolution non-hydrostatic Advanced Research WRF (ARW core) modeling system developed by the National Centre for Atmospheric Research (NCAR), USA, is considered. ARW dynamical core has an equation set which is fully compressible, Eulerian, and non-hydrostatic with a run-time hydrostatic option. Complete details of WRF ARW modeling system's equations, physics, and dynamics are described in Skamarock et al. (2008). Brief description of various schemes used for numerical simulations is given in the following sections.

3.1 Planetary boundary layer schemes

Unresolved turbulent vertical fluxes of heat, momentum, and moisture within the PBL are parameterized using closure PBL schemes (Stull and Driedonks 1987). Local closure schemes estimate the turbulent flows at each model grid point from the mean atmospheric variables and/or their gradients at that point, non-local closure schemes estimate the same fluxes at a given point using the mean profiles over the entire domain of turbulent mixing (Hu et al. 2010). Different PBL schemes Mellor-Yamada-Janjic (MYJ), Mellor-Yamada Nakanishi and Niino (MYN), and Yonsei University (YSU) scheme are considered; among them, MYJ and MYN are local closure models, whereas YSU is non-local model.

MYJ scheme is a turbulent-based model described by Mellor and Yamada (1982). It is a one-dimensional prognostic turbulent kinetic energy (TKE) scheme with local vertical mixing and use 1.5-order (level 2.5) turbulence closure model to represent turbulence above the surface layer. This scheme accounts for momentum and mass transfer by determining diffusion and turbulence locally. MYN is also 1.5-order turbulent closure model (Nakanishi and Niino, 2004). It is a TKE-based local mixing scheme. This scheme considers the non-local fluxes explicitly through a translucent term (Pleim and Chang 1992). YSU PBL scheme (Hong et al. 2006) is a first-order non-local scheme, with a counter gradient term in the eddy-diffusion equation. This scheme considers the non-local fluxes implicitly through a parameterized non-local term. It accounts momentum and mass transfer from large-scale eddies (Hong and Pan 1996), and has an explicit treatment for entrainment at the PBL top.

3.2 Microphysics

Microphysics parameterization scheme simulates the cloud life cycle by distributing water mass among multiple hydrometeor classes. Bulk microphysics schemes assume size distribution function for each hydrometeor type and predict one or more moments of that distribution. Different microphysics options considered are Thompson (THM), WRF single-moment 6-class (WSM), and Purdue Lin (LIN) schemes. In all the schemes, the six-class water substance includes the prognostic equations of mixing ratios of water vapour, cloud water, cloud ice, snow, rain, and graupel.

THM scheme is a bulk microphysics scheme based on Thompson et al. 2004. It assumes exponential particle size

distribution for all hydrometeors except snow follows linear combination of exponential and gamma distributions. It predicts the mixing ratios of five liquid and ice species: cloud water, rain, cloud ice, snow, and graupel, and also explicitly predicts the number concentration of cloud ice and rain drops. Thus, THM scheme is a two-moment scheme for cloud ice and rain water, and a one-moment scheme for all other condensate species (Thompson et al. 2008) and hence considered as hybrid scheme. WSM is a single-moment scheme from Hong et al. 2004 and predicts the mass mixing ratios of cloud water, cloud ice, snow, graupel, and rain, and all the hydrometeors follow exponential distribution. It incorporates new method for representing mixed-phase particle fall speeds for the snow and graupel by assigning single fall speeds to both particles and applying that fall speed to both sedimentation and accumulation processes (Dudhia et al. 2008). LIN scheme is based on Lin et al. (1983) and Rutledge and Hobbs (1984) with some modifications. The size distributions of the precipitating species are assumed to follow an exponential distribution. It is also single-moment scheme. This is a sophisticated scheme that has ice, snow, and graupel processes, including ice sedimentation and time split fall terms.

3.3 Cumulus parameterization schemes

Cumulus schemes are based on fundamental closure assumption in which convective effects are assumed to remove convective available potential energy (CAPE) in a grid element. Different schemes have different assumptions to explain the triggering mechanism and intensity of convection. Once cumulus schemes are triggered, the vertical profiles of grid column will be changed due to the modification of temperature and moisture profiles. Different cumulus schemes Kain Fritsch (KF), Betts Miller Janjic (BMJ), and Grells Devenyi Ensemble (GDE) are employed.

KF scheme (Kain 2004) is the update of its earlier parameterization (Kain and Fritsch 1993). The closure assumption in this scheme is based on the removal CAPE in a grid column within an advective time period. It triggers deep convection when a mixed parcel has positive vertical velocity over a depth that exceeds a specified cloud depth, typically 3–4 km (Kain et al. 2003). It is a mass flux scheme which determines the strength of convection from CAPE when deep convection is triggered. BMJ scheme is the extension of the Betts–Miller scheme (Betts and Miller 1986). It triggers convection when a parcel of air ascends a certain distance along with positive CAPE, similar in KF scheme. This scheme adjusts the atmospheric temperature and moisture profile towards the reference structures by including both deep and shallow convection. These

reference structures are pre-determined profiles of temperature and moisture inside the cumulus scheme. This scheme uses the thermodynamic profile that results from mixing of the convectively unstable layers to explain deep convection (Janjic 1994). GDE scheme makes use of ensemble parameterization with different closure assumptions and parameters (Grell and Devenyi 2002). To obtain the accurate precipitation amount statistically, these schemes determine the best configuration of ensemble of parameters and closure schemes by considering the triggering mechanisms, adjustment processes, and closure approximations from numerous schemes instead of using single cumulus scheme. A dynamic and trigger control is applied as a combination of 144 ensemble members. Closure assumption is based on CAPE, low-level vertical velocity, or moisture convergence for which quasi-equilibrium is applied for the available buoyant energy.

3.4 Experimental design

In this study, WRF with ARW dynamical core with model configuration consisting of one-way interactive triple-nested domains (horizontal resolution of 18, 6 and 2 km) and Lambert conformal map projection is used. The initial and boundary conditions for ARW model simulations are derived from National Centers for Environmental Prediction (NCEP) Global Forecast System (GFS) data of 00:00 UTC of 27th July 2011 available at $0.5^\circ \times 0.5^\circ$ resolution. An overview of nested model domain is shown in Fig. 4. Fifty-six vertical model levels are used with a vertical resolution of 50 m near surface, increasing to 100 m at 1.5 km, increasing to 250 m at 10 km level, and 500 m near the upper-model boundary at 30 km. Model configuration is given in Table 1. Various numerical experiments are carried out by changing the boundary layer, microphysics, and cumulus schemes. Summary of numerical

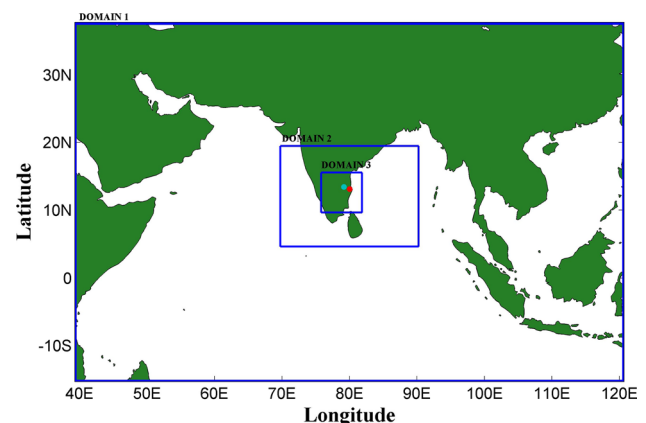


Fig. 4 Nested model domain used for numerical simulation; cyan and red solid circles in the figure correspond to study region and DWR sites

Table 1 Model configurations used for numerical simulation

WRF configuration	Description		
	Domain 1	Domain 2	Domain 3
WRF core	Advanced research WRF (ARW)	Advanced research WRF (ARW)	Advanced research WRF (ARW)
Spatial coverage	(40°E–120°E, 15°S–38°N)	(70°E–90°E, 5°N–20°N)	(76°E–82°E, 10°N–16°N)
Grid distance	18 km	6 km	2 km
Time step	60 s	30 s	10 s
Number of grid points	249 × 271	223 × 223	223 × 223
Vertical levels	56	56	56
Initial and boundary conditions	NCEP GFS (0.5 × 0.5)	NCEP GFS (0.5 × 0.5)	NCEP GFS (0.5 × 0.5)
Long-wave radiation	RRTM Scheme	RRTM Scheme	RRTM Scheme
Short-wave radiation	Dudhia Scheme	Dudhia Scheme	Dudhia Scheme
Dynamic option	Eulerian Mass	Eulerian Mass	Eulerian Mass
Map projection	Lambert conformal	Lambert conformal	Lambert conformal

experiments conducted is provided in Table 2. In the third domain which is run at 2 km spatial resolution, simulations are carried out using explicit convection. For radiation, the Rapid Radiative Transfer Model (RRTM) long-wave radiation (Mlawer et al. 1997) and Dudhia short-wave radiation schemes (Dudhia 1989) are adopted, and are left unchanged for all the runs.

4 Results and discussions

4.1 Sensitivity to boundary layer parameterizations

To assess the ability of model simulations in replicating the key features in PBL, model simulated surface features are compared with ISRO AWS observations (145 in number). Model simulated 2-m temperatures at 13:00 UTC on 27th July 2011 over the third domain along with the AWS temperatures are shown in Fig. 5a–c. Time 13:00 UTC corresponds to convective initiation over study region. Model simulations from three different PBL schemes show slightly warmer temperatures during the convective initiation (13:00 UTC) similar to AWS observations. To assess

the general performance of boundary layer schemes, domain wide statistics is carried out for domain 3. Spatial correlation between model simulated values and AWS observations is calculated by interpolating model grid points to the nearest observations. Correlation coefficients for respective schemes are shown at low-right corner of Fig. 5a–c. Even though significant differences are not noticed between correlation values for different schemes, MYJ is showing relatively better correlation of 0.74 compared to the other schemes; all the correlations obtained are significant at 95% level. Point-wise absolute model error (absolute value of model minus observations) is also calculated. In this case, the number of valid pairs (N) is one, since correlations are calculated at each station separately. For MYJ scheme, it is noticed that the absolute model error is relatively less at almost all the grid points (solid circles in Fig. 5d–f). Correlation between model-derived values and observations for various parameters is given in Table 3. Higher correlation coefficients in MYJ scheme for 2-m temperature (T_{2m}), 2-m potential temperature (θ_{2m}), and wind speed at 10 m (ws_{10m}) indicate a better performance of MYJ scheme in simulating the near surface meteorological variables.

One possible cause for differences in simulation of T_{2m} from different PBL schemes could be due to differences in boundary layer height produced by different schemes. To investigate this, boundary layer height is calculated using temperature and moisture profiles obtained from respective schemes and MWR observations over Gadanki grid point. To eliminate formulation dependence of different approaches in different PBL schemes, height of PBL is calculated using virtual temperature (Stull 1988). Figure 6a illustrates the temporal evolution of PBL height simulated from different PBL schemes along with MWR. Temporal evolution of PBL height from MWR observations shows deep PBL

Table 2 Summary of various numerical experiments

Cumulus	Microphysics	Boundary layer
GDE	THM	MYJ
KF	THM	MYJ
BMJ	THM	MYJ
BMJ	LIN	MYJ
BMJ	WSM	MYJ
BMJ	THM	YSU
BMJ	THM	MYN

Fig. 5 Spatial distribution of WRF simulated 2-m temperature over domain 3 at 13:00 UTC of 27th July 2011 from different PBL schemes (a MYJ, b MYN, and c YSU). AWS observations are mapped with solid circles (top panel). Correlation coefficient (R) is given at bottom-right corner of top panels. Absolute error values (K) between observations and different PBL schemes are shown at bottom panels (d MYJ, e MYN, f YSU)

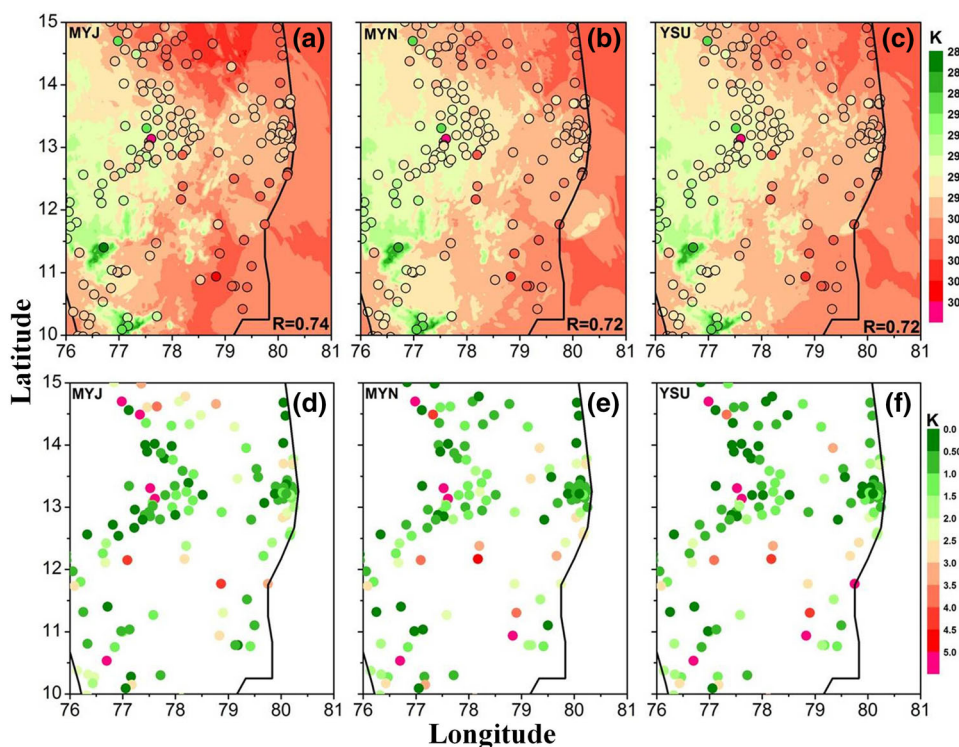


Table 3 Correlation between AWS and PBL simulations at 13:00 UTC of 27th July 2011

Scheme	R		
	T_{2m}	θ_{2m}	ws_{10m}
MYJ	0.74	0.19	0.19
MYN	0.72	0.04	0.09
YSU	0.73	0.06	0.18

height during the storm initiation (13:00UTC) over the study region (Fig. 6a). Among the three PBL schemes, MYJ simulates the highest PBL at 13:00UTC similar to observations. MYN simulated PBL height is lower than MYJ and also no significant increase is noticed during the storm initiation. In contrast, YSU scheme has showed decrease in PBL height around 13:00 UTC which clearly reveals that storm initiation is not at all captured in YSU scheme. Since the height of PBL is based on stability of the atmosphere, temperature and moisture profiles within boundary layer are analyzed. Potential temperature (θ) and moisture profiles at 13:00 UTC from different schemes along with MWR observations are shown in Fig. 6b and c. Significant variations are noticed in vertical structure of potential temperature. For instance, MYJ simulates high temperature and low moisture below 2 km and low temperatures and high moistures above 2 km when compared to MWR observations. However, the other two schemes show low temperatures and high moistures at all levels when compared with MWR. This implies that MYJ scheme is able to produce sufficient amount of heat and

moisture from surface and resulting in vertical transport of heat and moisture into the PBL. In contrast, the other two schemes predict relatively low temperature at the surface which might have resulted in less heat transport. However, there are differences in MYJ simulated vertical profiles of temperature and moisture when compared to MWR observations as bias of the instrument is not taken into consideration (Madhulatha et al. 2013).

It is inferred that among three PBL schemes, MYJ predicts highest PBL compared to other schemes MYN and YSU during storm initiation. Differences in vertical mixing may be the reason for differences in PBL height. Stronger vertical mixing in MYJ could be the reason for stronger entrainment at the top of PBL which, perhaps, produced warm PBL. Although, MYN and MYJ, both are local schemes, the simulation of PBL is different in both the schemes. One-dimensional prognostic TKE scheme in MYJ could be the possible reason for better simulation of local vertical mixing which might have resulted in simulating warm surface temperatures. On the other hand, YSU is a non-local closure model which is different from the other two schemes. For the present case, MYJ local closure scheme performed well in simulating the surface parameters by accounting local entrainment. More detailed picture can be obtained by repeating the analysis over all grid points, but, because of unavailability of observations, the present analysis is limited only to Gadanki grid point. Overall results showed that MYJ scheme showed a better performance compared to other schemes in capturing the various surface parameters.

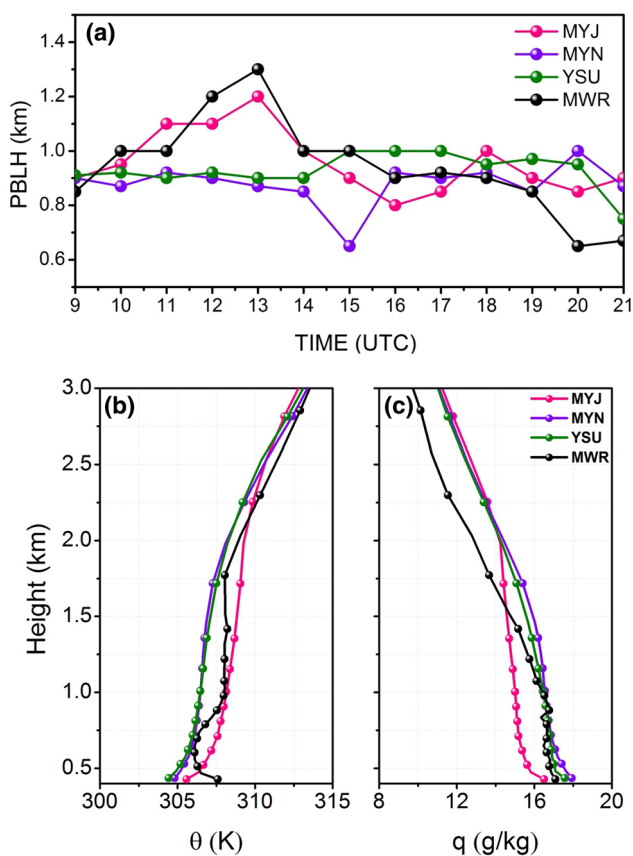


Fig. 6 a Time evolution of PBL height (km), vertical profiles of b potential temperature (K), c specific humidity (g/kg) at 13:00 UTC of 27th July 2011 over Gadanki from MWR and different PBL schemes

4.2 Sensitivity to cloud microphysics parameterization

As microphysics parameterization scheme simulates the cloud life cycle by distributing water mass among multiple hydrometeors classes, to understand the effectiveness of different microphysics schemes, reflectivity is examined, since it is a function of cloud hydrometeors. Spatial distribution of reflectivity at 15:00 UTC of 27th July 2011 from model simulations along with DWR observations is shown in Fig. 7. To account all types of hydrometeors, the time 15:00 UTC which corresponds to mature phase of the storm is considered. For comparison, DWR observations are gridded to model resolution 2 km. Associated with the formation of MCS over south-east India, high reflectivity values (>30 dBz) are observed surrounding Gadanki region (black square rectangle) and system is oriented east of study region (Fig. 7a). THM scheme is able to capture the magnitude of reflectivity associated with MCS as seen in observations; however, the system is oriented towards south compared to observations (Fig. 7b). In contrast, the simulated reflectivity from LIN and WSM schemes

distributed more towards south and south-west region. Area averaged bias and RMSE between observed and simulated reflectivity for domain 3 show that all simulations are underestimating reflectivity when compared to DWR observations; however, THM scheme showed less BIAS and RMSE compared to other schemes (Table 4).

As model simulated reflectivity is dependent on hydrometeors, the possible reasons for differences in simulated reflectivity could be due to different assumptions in microphysical schemes. As simulation proceeds, each microphysical scheme redistributes the total mass of atmospheric water among different phases. Since the fundamental differences among all cloud microphysics schemes are the magnitudes and distributions of hydrometeors, it is desirable to examine the evolution of cloud hydrometeors in different numerical experiments. Figure 8 compares the time evolution of area averaged total column integrated cloud water (Q_{clid}), rainwater (Q_{ran}), cloud ice (Q_{ice}), snow (Q_{snw}), and graupel (Q_{grp}) from all simulations. Substantial differences are noticed between different simulations in distribution of hydrometeors. As the simulation proceeds, THM scheme redistributes atmospheric water content as high amounts of cloud, intermediate amounts of rain, low ice, high snow, and low graupel; LIN scheme simulates intermediate cloud, low rain, moderate ice, low amounts of ice, and intermediate graupel; WSM scheme simulates low cloud, high amounts of rain, high amounts of ice, intermediate snow, and high graupel at 15:00 UTC.

To investigate the contribution of each of these hydrometeors in simulating reflectivity, stacked bar plot of the hydrometeors is plotted (Fig. 9a). As model simulated reflectivity is a function of precipitating hydrometeors rain, snow, and graupel (Stoelinga et al. 2005), only these three hydrometeors are examined along with water vapour mixing ratio. Among the three hydrometeors, rainwater has high reflectivity values followed by graupel and snow. THM scheme simulated high amounts of Q_{ran} followed by WSM and LIN (Fig. 9a). The amount of rainwater within a column is a function of fall speed of the droplets. Basically, faster the fall speeds, lower the rainwater mixing ratio, as rainwater leaves the column more rapidly (Otkin et al. 2006). THM scheme showed large rain water mixing ratio as it might have simulated smaller droplets with slower fall speeds. Relatively less amounts of rain mixing ratios are produced by LIN and WSM. THM scheme generates large amounts of snow followed by WSM and LIN. Fewer amounts of graupel mixing ratio are produced by THM scheme, whereas intermediate and higher amounts of graupel are simulated in LIN and WSM schemes, respectively. On an average, among all the schemes THM scheme simulated more rain water, more snow and less graupel (Fig. 9a), large mixing ratio (Fig. 9b), so the

Fig. 7 Spatial distribution of reflectivity (dBz): **a** DWR, **b** THM, and **c** WSM at 15:00 UTC of 27th July 2011

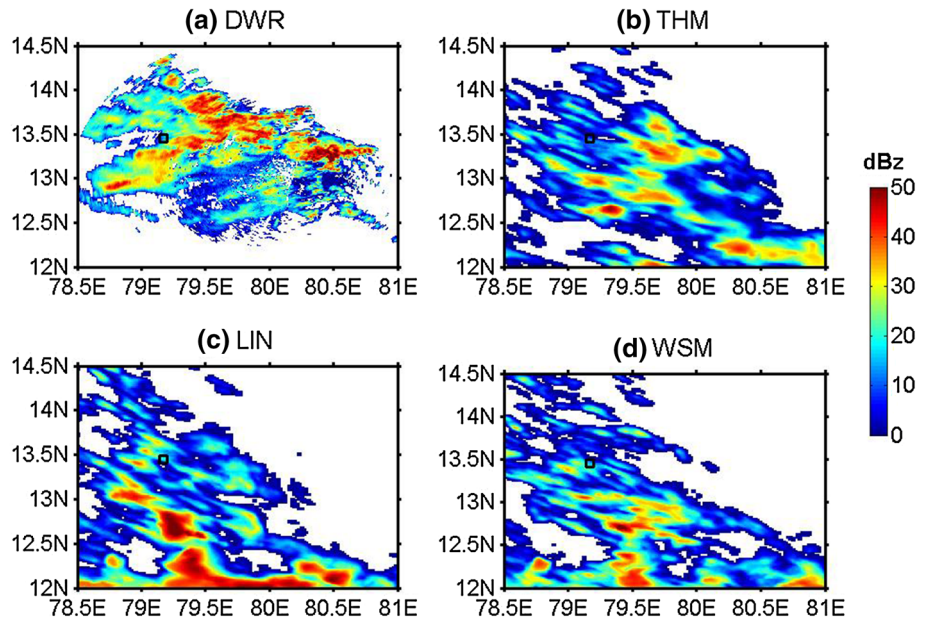


Table 4 Domain wide statistics of reflectivity between DWR and microphysics simulations at 15:00 UTC of 27th July 2011

	Average reflectivity (dBz)	Maximum reflectivity (dBz)	Bias	RMSE
DWR	13.05	56.45	–	–
THM	7.63	48.06	5.42	2.32
LIN	6.17	54.16	6.88	2.62
WSM	5.71	52.99	7.35	2.71

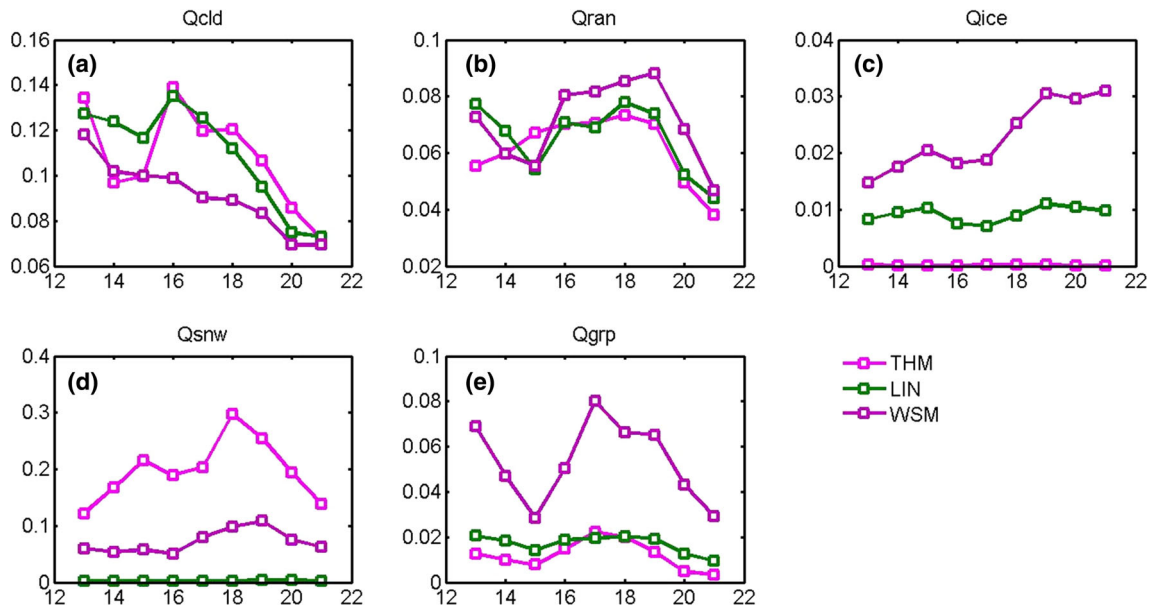


Fig. 8 Time series of area averaged and column integrated cloud hydrometeors (g/kg) from different microphysics schemes on 27th July 2011. **a** Qcld, **b** Qran, **c** Qice, **d** Qsnw, and **e** Qgrp

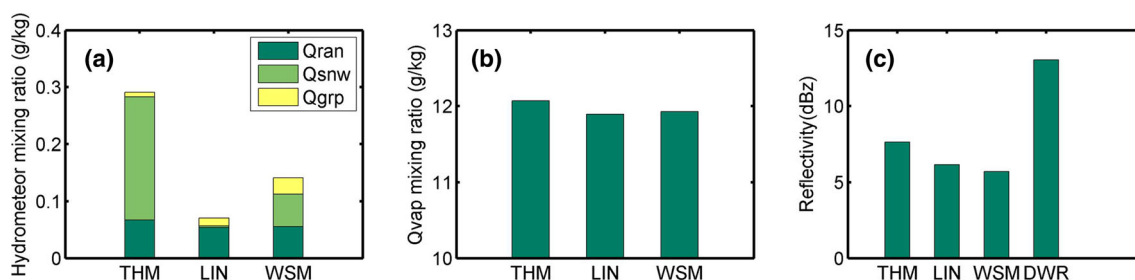


Fig. 9 Stacked bar diagram of different hydrometeors; bar diagram of **b** Qvap (g/kg) and **c** reflectivity (dBz)

quantitative contribution of all these hydrometeors might have resulted in simulating high reflectivity (Fig. 9c) compared to other schemes. LIN scheme generated intermediate rain water, low snow, and intermediate graupel amounts; as a result, the integrated effect of these three hydrometeors might have produced intermediate reflectivity. WSM scheme produced intermediate amounts of rain and snow, high amounts of graupel which could have resulted in simulating low reflectivity values.

From this analysis, it is inferred that the performance of THM scheme is better than the other two schemes. Differences in distribution of hydrometeors could be the reason for differences in reflectivity simulations. THM scheme which accounts both mixing ratio and number concentration for rainwater might have contributed for better simulation of reflectivity. On the other hand, the other two schemes which account only the mixing ratio of rain water might have affected the simulation of reflectivity. This could be the one possible reason for a better performance of THM scheme in simulating reflectivity. However, direct measurements of cloud hydrometeors are crucial for further investigation. Numerous considerations like ground clutter, anomalous propagation, and bright bands of DWR (Hubbert et al. 2009) are not taken into consideration. This may be also a reason for the large discrepancies between observed and model simulated reflectivity.

4.3 Sensitivity to cumulus parameterization

Sensitivity of model simulations to cumulus schemes is investigated by examining precipitation. Since model runs are carried out with explicit convection in the third domain, precipitation simulations in second domain are considered for present analysis. Figure 10 shows model simulated and observed 24-h accumulated precipitation. For comparison, model simulated rainfall is integrated to GsMAP spatial resolution. Intense rainfall (>35 mm) between 13°N and 14°N and off-shore the coast is evident in observations; an east–west orientation of the convective system is also apparent (Fig. 10a). BMJ scheme (Fig. 10b) is able to capture the rainfall pattern reasonably well as in

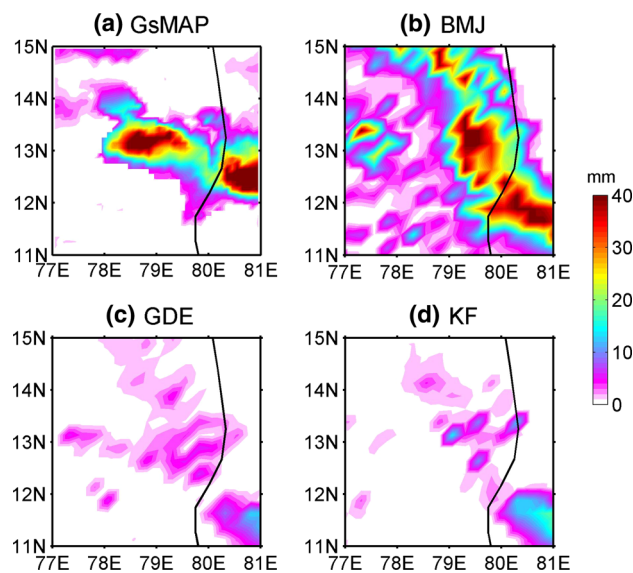


Fig. 10 Spatial map of 24-h accumulated rainfall for 27th July 2011 from different cumulus schemes: **a** BMJ, **b** GDE, **c** KF, and **d** GsMAP observations

observations (Fig. 10a) besides a spatial shift along the latitude direction and differences in the orientation of cell main axis are noticed. The other two schemes, GDE and KF (Fig. 10c, d), largely underestimated the rainfall. Both the schemes exhibit low rainfall over most of the domain. Domain wide statistics for precipitation is also carried out by interpolating model grid points nearest to observations. Table 5 summarizes precipitation characteristics for observed data along with model simulated precipitation which shows both GDE and KF simulations largely underestimate precipitation. On the other hand, BMJ scheme estimated the domain averaged precipitation and maximum rainfall amounts reasonably well with respect to observations. BIAS and RMSE are smaller in BMJ scheme compared to GDE and KF schemes (Table 5).

BMJ produced more realistic representation of surface precipitation. One possible cause for the differences in rainfall simulations may be the differences in treatment of vertical redistribution of heat, moisture, and momentum by each scheme which play vital role in explaining the vertical instability of the atmosphere. To inspect this, Convective

Table 5 Domain wide statistics of 24-h accumulated precipitation between GsMAP and cumulus simulations

	Average reflectivity (dBz)	Maximum reflectivity (dBz)	Bias	RMSE
GsMAP	7.84	82.2	–	–
BMJ	8.8	76.8	1.04	1.01
GDE	1.23	23.6	–6.58	2.55
KF	1.24	54.5	–6.59	2.56

Available Potential energy (CAPE) over Gadanki grid point simulated from different cumulus schemes is analyzed and compared with the collocated MWR observations. Time evolution of CAPE from different schemes and MWR is shown in Fig. 11a. In the pre-environment of the storm around 12:00 UTC increase in CAPE is clearly noticed in all the schemes. Around 13:00 UTC, MWR observations showed maximum CAPE which is an important precursor for the storm initiation and is clearly brought out in BMJ scheme. Gradual decrease in CAPE is observed after 13:00 UTC associated with the release of energy due to precipitation fall out. Similar variations in CAPE associated with convection over Gadanki region are reported by Mohan and Rao 2012. This is well simulated in BMJ scheme than the other two schemes. Temporal variation and intensity of CAPE simulated by BMJ scheme is in close agreement with MWR observations. This might be the reason for better simulation of rainfall in BMJ scheme.

It is inferred that CAPE simulated by BMJ is matching well with the observations. The reason could be the

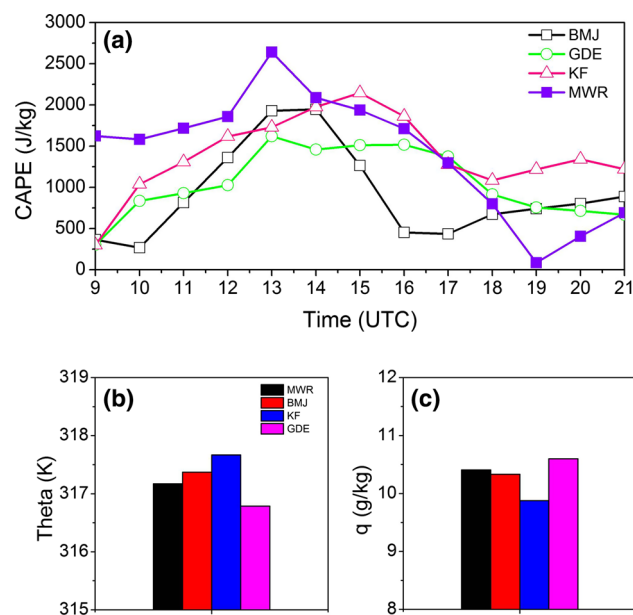


Fig. 11 a Time evolution of CAPE; bar diagram of b theta (K) and c specific humidity (g/kg) averaged from surface to 300 hPa at 13:00 UTC of 27th July 2011 over Gadanki from MWR observations and different cumulus schemes

different adjustment process used in different schemes in adjusting the model thermodynamic soundings. To calculate CAPE, BMJ scheme attempts to adjust the model sounding to a pre-determined reference profile, whereas KF scheme considers the model sounding and GDE scheme adjusts the model thermodynamic profiles from mean feedback of ensemble schemes. For the same model simulated profile, BMJ scheme adjusts to pre-determined reference profile which is based on climatology and the amount of latent heat released might be sufficient to produce the realistic CAPE which might have created the unstable atmosphere necessary to trigger convection. KF scheme which uses the model sounding to initiate convection might not have able to produce realistic latent heat and in turn necessary CAPE for strong convection to occur. The GDE scheme which is the ensemble of many schemes, adjusted the model profile to some extent, which could not have produced enough latent heat and large CAPE to trigger strong convective environment. Results are consistent with Pennelly et al. (2014).

To evaluate the simulated thermodynamic profiles produced by different schemes, layer averaged potential temperature and moisture from surface to 300 hPa at 13:00 UTC is compared with MWR observations (Fig. 11b, c). BMJ produced layer averaged potential temperature and moisture are showing close agreement with MWR, whereas KF is producing warmer and drier atmosphere and GDE is simulating cooler and drier atmosphere when compared with observations. Better performance of BMJ scheme can be attributed to proper representation of unstable atmosphere in storm environment by adjusting thermodynamic profiles to reference profiles. More detailed information can be obtained by repeating the analysis over all the grid points as the present inspection is only attributed to Gadanki grid.

5 Simulation with better combination of physical schemes

From the above analysis, it is clear that BMJ cumulus scheme, MYJ PBL scheme, and THM microphysics scheme showed better performance in simulating various

MCS features. Using this combination of parameterization schemes, a numerical simulation is carried out and results are compared with different available in situ observations over Gadanki.

5.1 System evolution

Time-height cross section of reflectivity derived from the model simulation is compared with DWR observations over Gadanki grid point (Fig. 12). Associated with passage of MCS, a weak convective cell with reflectivity 20 dBz is observed around 12:00 UTC (Fig. 12a). Later, multi-cell structure with two intense cells around 13:00 UTC and 15:00 UTC with reflectivity around 45 dBz and maximum vertical extent up to 7 km. Model simulation showed convective initiation around 11:30 UTC with slightly high reflectivity around 30 dBz. Multi-cell structure of storm is also noticed (Fig. 12b). However, there are differences in timing and vertical distribution of storm. High reflectivity values (>50 dBz) and low vertical extents are simulated compared to observations. Well-organized structure of system is not very clear in simulation. Even though discrepancies are noticed between observations and simulations, WRF model is able to simulate the convective initiation and propagation of MCS over the study region.

5.2 Surface features

Hourly surface parameters from AWS located at Gadanki along with model simulated values are shown in Fig. 13. Passage of storm is accompanied by sudden drop in temperature (T) (cooling) and increase in relative humidity (Rh) (Fig. 13a, b). Rapid cooling around 5 °C and increase in Rh by ~50% are noticed. Model simulated surface temperature and Rh are in agreement with AWS

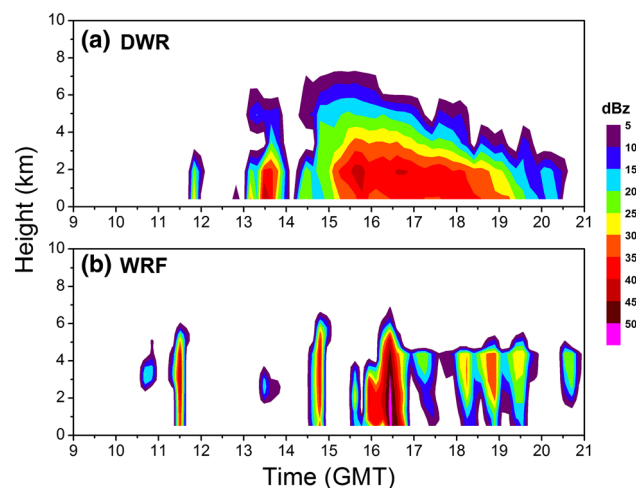


Fig. 12 Time-height cross section of reflectivity on 27th July 2011 over Gadanki: **a** DWR and **b** WRF

observations. Observations shows temperature drop from 31 to 25 °C, whereas WRF simulation shows drop from 32 to 25 °C. Observed Rh values rise from 50 to 90%, whereas the model shows a sharp rise from 40 to 95% (Fig. 13b). A rapid increase in surface pressure (Ps) of ~3 hPa is seen in both observations and simulations (Fig. 13c), which indicates the meso-high associated with the storm (Rajeevan et al. 2010). Sharp increase in wind speed (Ws) and change in wind direction (Wd) are clear. Observed wind speed rises from 2 m/s to 5 m/s, whereas model wind speed rises from 4 to 8 ms⁻¹ and shift in wind direction is also evident (Fig. 13d, e). Rainfall is reported in both observations (~15 mm) and model (~35 mm) (Fig. 13f). However, all these variations are noticed around 13:00 UTC for AWS and around 12:00 UTC for the model, temporal shift is clearly apparent. It is noticed that model is able to capture the variations in surface meteorological features associated with storm besides biases in terms of intensity and timing.

5.3 Vertical structure

Vertical profiles of different meteorological parameters derived from model and GPS sonde at 12:00UTC are presented in Fig. 14. Model and observed temperatures from surface to 300 hPa show good agreement in magnitude; however, large differences of around 5–10 °C are observed at higher altitudes (above 300 hPa). Close match is seen for Rh at lower levels (up to 850 hPa); between 850 and 700 hpa slight differences of about 10%; between 700 and 500 hpa differences of about 20% are noticed. Large differences of about 30–40% in Rh are evident between 400 and 200 hPa levels. Wind speed profiles follow relatively a similar pattern. However, the model shows relatively intense winds of about 4–5 m/s at lower levels and higher levels (around 200 hPa). In terms of wind direction, reasonably good matching is noticed. GPS profiles show northwesterlies at the lower levels and wind reversal around 500 hpa, and similar features are replicated in the model, besides wind reversal is evident around 400 hPa. It is noticed that vertical profiles of temperature, moisture, and wind speed and wind direction are reasonably well simulated with slight variations. Various stability parameters CAPE, LCL (Lifting Condensation level), and LFC Level of Free Convection), KI and LI (Lifted Index), etc., are calculated from the GPS soundings (Table 6). Thermodynamic analysis of GPS sonde indicates large values of CAPE ~850 J kg⁻¹ and small values of CIN ~-13 J kg⁻¹ explaining the favourable environment for severe weather. Negative values of LI, and high values of other indices KI, HI, TTI explain the potential for storm initiation (Table 6). Model-derived stability indices also showed favourable environment for severe weather.

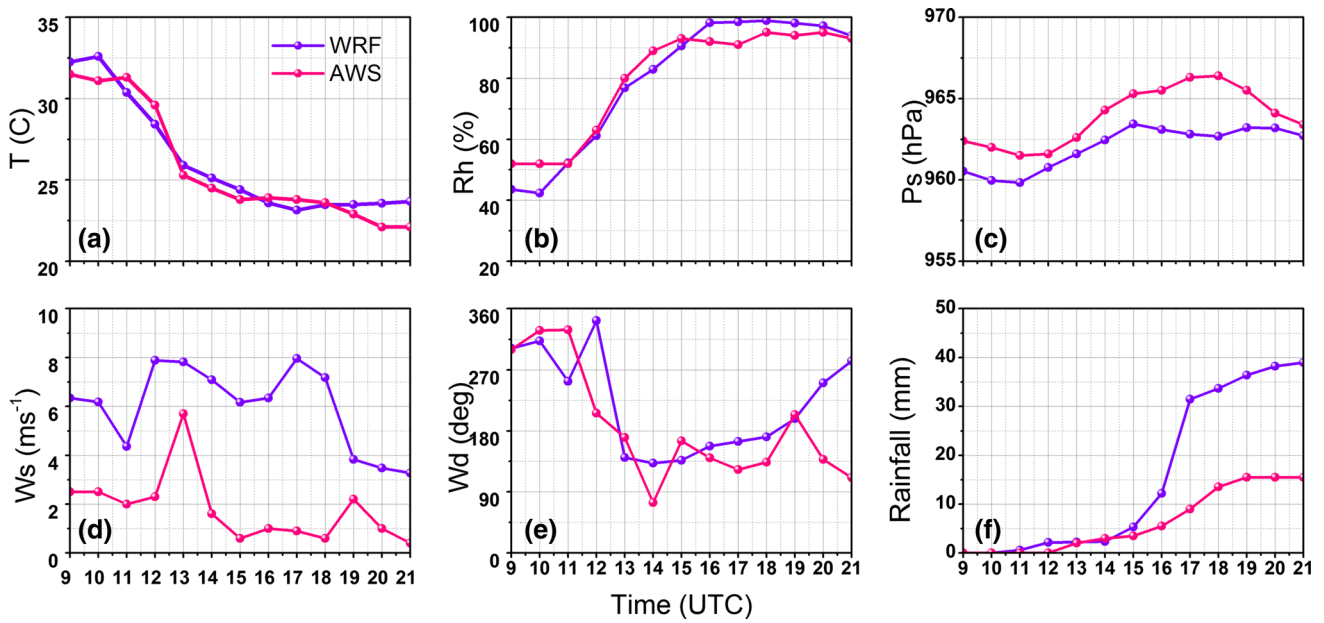


Fig. 13 Hourly observations of various meteorological parameters over Gadanki on 27th July 2011 from AWS and WRF simulation

Fig. 14 Vertical profiles of various meteorological parameters at 12:00 UTC of 27th July 2011 over Gadanki from GPS and WRF simulations: **a** T(C), **b** Rh (%), **c** Ws (ms⁻¹), and **d** Wd (deg)

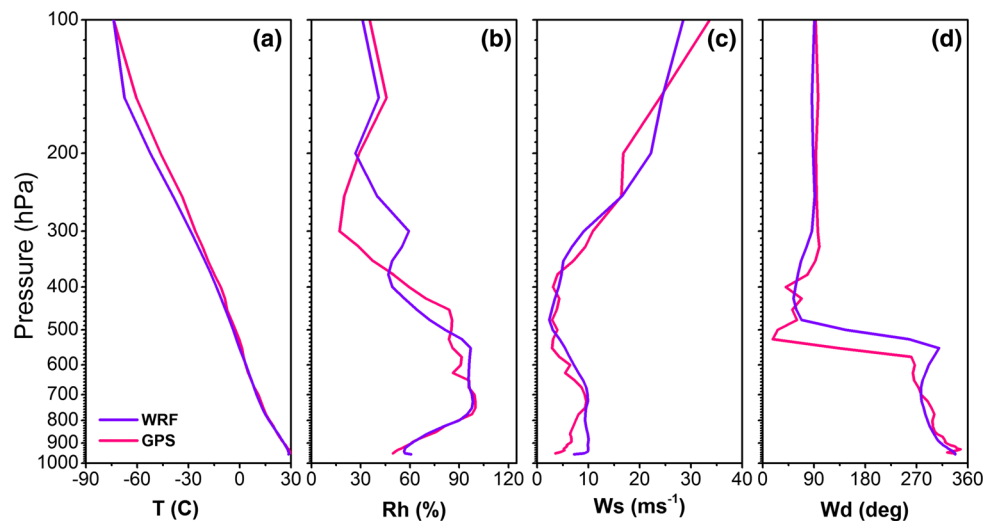


Table 6 Stability indices from GPS sonde and WRF at 12:00 UTC of 27th July 2011

Index	GPS	WRF
CAPE(J/kg)	858	4119
CIN(J/kg)	-13	-34
LI	-2	-4.2
KI	41.9	41.3
TTI	45.9	47.6
SWEAT	244.1	243.5

5.4 Thermodynamic structure

Time-height cross sections of temperature and vapour density within lower troposphere from MWR and model are shown in Figs. 15 and 16, respectively. Increase in

temperature and vapour density within the boundary layer during the initiation of the storm and relative decrease of these parameters after storm dissipation are observed (Figs. 15 and 16). Raise in temperature is observed from surface to 750 hPa in MWR, with surface temperatures around 304 K (Fig. 15a). Model simulated values also show raise in temperatures, besides warmer surface temperatures (>304 K) are simulated (Fig. 15b). Variations in temperature from surface to lower troposphere (750 hpa) are associated with the condensation and evaporation processes occurring during the storm evolution. MWR observations show increase in vapour density from surface to 750 hpa level during the storm passage (Fig. 16a). Model simulations also show increase in vapour density; however,

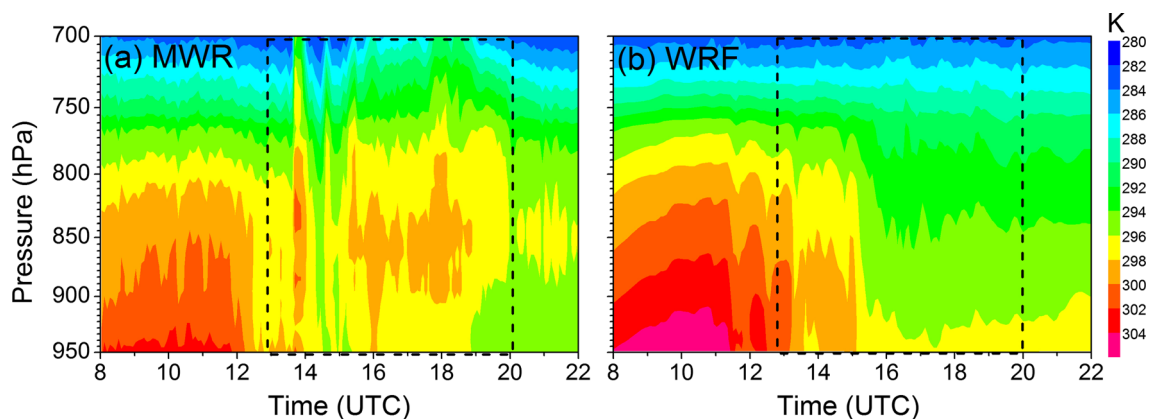


Fig. 15 Time-height cross section of temperature on 27th July 2011 over Gadanki: **a** MWR and **b** WRF simulations; duration of the storm is shown in *dotted line*

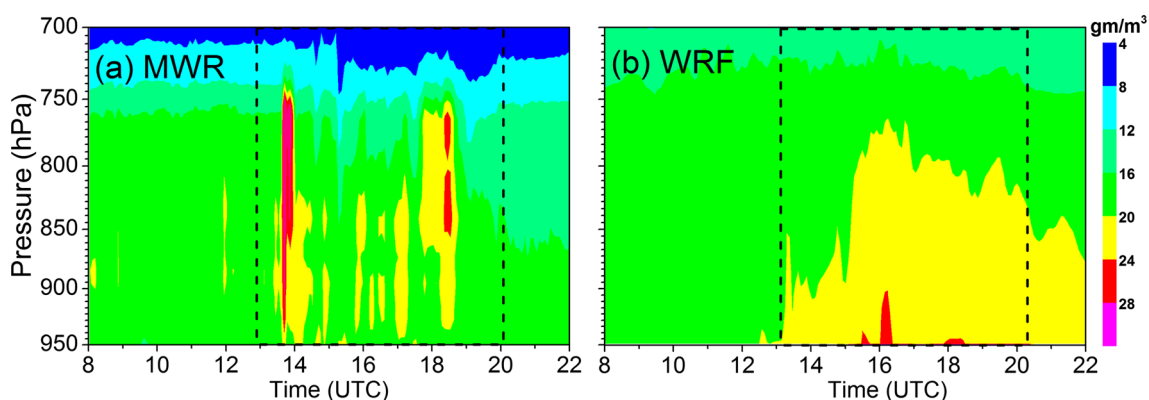


Fig. 16 Time-height cross section of vapour density on 27th July 2011 over Gadanki: **a** MWR and **b** WRF simulations; duration of the storm is shown in *dotted line*

less moisture is simulated both at surface and different levels (Fig. 16b). The presence of moisture and warm temperatures which are the basic storm formative mechanisms is clearly noticed both in observations and simulations with variations in intensity and timing.

6 Conclusions

In this study, the impact of various PBL, microphysics, and cumulus parameterization schemes on simulation of mesoscale convective system is examined. Series of experiments are performed with the WRF model using three nested domains to compare the sensitivity of simulation of MCS occurred over south-east India on 27th July 2011. Three different treatments of PBL schemes (MYN, MYJ, and YSU); microphysics (THM, LIN, and WSM) and cumulus convection (BMJ, KF, and GDE) are considered for numerical simulations. All the model runs are initialized using GFS data. Performances of different schemes are examined by comparing with the available (ISRO

AWS, GSMAP, and DWR) observations. Warm temperatures associated with convective initiation, reflectivity, and rainfall patterns of MCS are well simulated by MYJ, THM, and BMJ schemes, respectively. Domain wide statistics revealed that these schemes showed high correlation, less bias, and RMSE in respective considered parameters. Physical explanations for differences between the schemes are explored by examining boundary layer height, distribution of hydrometeors, and instability parameters by validating with observations. Among the PBL schemes, MYJ simulated warm temperatures necessary for storm initiation by simulating strong mixing essential to produce high PBL. Local closure TKE in MYJ scheme might have contributed to realistic representation of mixing in the boundary layer and better simulation of surface features in the storm environment. Among the microphysics schemes, THM simulated the reflectivity associated with MCS reasonably well. Inclusion of both number concentration and mixing ratio of raindrops in THM hybrid moment scheme could be the reason for proper representation of different hydrometeors and better simulation of reflectivity.

Among the cumulus schemes, BMJ has performed well in simulating precipitation. BMJ closure scheme, which adjusts thermodynamic profiles to the reference climatological profiles, perhaps, resulted in proper representation of CAPE and contributed to better precipitation simulation. Analysis suggests that, for this particular case study, BMJ (closure cumulus scheme), MYJ (local closure turbulent boundary layer scheme), and THM schemes (a six-class hybrid moment microphysics scheme) have performed better. With this combination of parameterization schemes, a new simulation is conducted. Resulting model simulation is able to capture initiation, propagation, surface features, and thermodynamic structure and precipitation features of MCS reasonably well with slight variations in location, timing, and intensity.

This study demonstrates that PBL schemes influence the simulation of surface characteristics; microphysics affect hydrometeor distribution (reflectivity); and cumulus convection controls the rainfall simulation, respectively. However, this study has certain limitations which need to be further investigated. To understand the underlying reasons of performance differences for PBL and microphysics schemes, different parameters are analyzed only over Gadanki grid point due to non-availability of data over all the grid points. And also, no direct observations are available to compare model simulated cloud hydrometeors from different microphysics schemes. Direct measurements of cloud hydrometeors are essential to investigate the complex microphysical processes. Therefore, there is a need of meso observation network to understand the broad picture of different fine-scale physical processes associated with life cycle of severe convective systems (Rajeevan et al. 2010). Current study is limited to only one event; to generalize the results discussed here, more number of cases have to be considered. For performing numerical simulations, only few cumulus (BMJ, GDE, and KF), microphysics (THM, LIN, and WSM), and PBL (MYJ, MYN, and YSU) schemes are selected based on different convective adjustments, distributions of cloud hydrometeors, and closure assumptions of respective schemes. However, to understand the robustness of the available schemes, more simulations have to be conducted. In addition, interactions between different physical schemes play significant role in simulation of various MCS features (Jankov et al. 2005) which needs to be further examined. Differences between simulations and observations noticed in the current results can also be due to uncertainties in different physical schemes, initial conditions, and interactions between different components of the model (Wu et al. 2013). All these issues are aimed in our future study.

In conclusion, improving the simulation of MCS remains a very challenging problem, even though the NWP models are equipped with sophisticated subgrid-scale schemes.

Modifying the parameterization schemes with improved understanding of physical processes with variety of observations can significantly help to improve the simulation of MCS. However, this study is intended to be first step in gaining the understanding of different physical schemes. Overall, current work demonstrates that the choice of parameterization schemes can influence model results and impact the simulation of severe convective events.

Acknowledgements We are thankful to scientific data centers NCEP, GES DISC, JAXA, and ISRO. WRF USERS page is greatly acknowledged for making the WRF model freely accessible to the user community. This research was funded by National Atmospheric Research Laboratory (NARL) under the Junior Research Fellowship (JRF) program sponsored by Department of Space (DOS), India. The first author was funded to carry out her Ph.D. thesis work under this program. Authors gratefully acknowledge Dr A. Jayaraman, Director NARL for his support and encouragement in providing High Performance Computing facilities and necessary observations to carry out this work. Special thanks to Dr. S.B. Thampi of Doppler Weather Radar Division, India, Meteorological Department (IMD), Chennai, India for providing DWR data. The in situ observations and DWR data utilised in this study can be available on special request at <http://www.narl.gov.in> and <http://www.imd.gov.in> respectively. We would like to thank two anonymous reviewers and editor for their helpful suggestions.

References

- Abhilash S, Mohankumar K, Das S (2008) Simulation of microphysical structure associated with tropical cloud clusters using mesoscale model and comparison with TRMM observations. *Int J Remote Sens* 29:2411–2432
- Arakawa A, Schubert WH (1974) Interaction of a cumulus cloud ensemble with the large-scale environment. Part I. *J Atmos Sci* 31:674–701
- Betts AK, Miller MJ (1986) A new convective adjustment scheme. Part II: single column tests using GATE wave, BOMEX, ATEX and arctic air mass data sets. *Q J Roy Meteor Soc* 112:693–709
- Chatterjee P, Pradhan D, De UK (2008) Simulation of hailstorm event using Mesoscale Model MM5 with modified cloud microphysics scheme. *Ann Geophys* 26:3545–3555
- Cintineo R, Otkin JA, Xue M, Kong F (2014) Evaluating the performance of planetary boundary layer and cloud microphysical parameterization schemes in convection-permitting ensemble forecasts using synthetic GOES-13 satellite observations. *Mon Weather Rev* 142:163–182
- Cohen AE, Cavallo SM, Coniglio MC, Brooks HE (2015) A review of planetary boundary layer parameterization schemes and their sensitivity in simulating Southeastern US cold season severe weather environments. *Weather Forecast* 30:591–612
- Coniglio MC, Correia J Jr, Marsh PT, Kong F (2013) Verification of convection-allowing WRF model forecasts of the planetary boundary layer using sounding observations. *Weather Forecast* 28:842–862
- Deb SK, Kishtawal CM, Bongirwar VS, Pal PK (2010) The simulation of heavy rainfall episode over Mumbai: impact of horizontal resolutions and cumulus parameterization schemes. *Nat Hazards* 52:117–142. doi:10.1007/s11069-009-9361-8
- Dudhia J (1989) Numerical study of convection observed during the winter monsoon experiment using a mesoscale two-dimensional model. *J Atmos Sci* 46:3077–3107

- Dudhia J, Gill D, Manning K, Wang W, Bruyere C (2002) PSU/NCAR Mesoscale Modeling System (MM5 version 3) tutorial class notes and user's guide. National Center for Atmospheric Research, Boulder, Colorado, USA
- Dudhia J, Hong SY, Lim KS (2008) A new method for representing mixed-phase particle fall speeds in bulk microphysics parameterizations. *J Meteorol Soc Jpn* 86A:33–44
- Fabry F (2006) The spatial variability of moisture in the boundary layer and its effect on convection initiation: project-long characterization. *Mon Weather Rev* 134:79–91
- Fadnavis S, Deshpande M, Ghude SD, Raj PE (2014) Simulation of severe thunderstorm event: a case study over Pune, India. *Nat Hazards* 72:927–943
- Ferreira JA, Carvalho AC, Carvalho L, Rocha A, Castanheira JM (2014) On the influence of physical parameterisations and domains configuration in the simulation of an extreme precipitation event. *Dynam Atmos Oceans* 68:35–55
- Flaounas E, Bastin S, Janicot S (2011) Regional climate modelling of the 2006 West African monsoon: sensitivity to convection and planetary boundary layer parameterisation using WRF. *Clim Dynam* 36:1083–1105
- Gilliland EK, Rowe CM (2007) A comparison of cumulus parameterization schemes in the WRF model. In: Proceedings of the 87th AMS Annual Meeting and 21th Conference on Hydrology (Vol. 2)
- Grell GA, Devenyi D (2002) A generalized approach to parameterizing convection combining ensemble and data assimilation techniques. *Geophys Res Lett* 29:14
- Hong SY, Pan HL (1996) Nonlocal boundary layer vertical diffusion in a medium-range forecast model. *Mon Weather Rev* 124:2322–2339
- Hong SY, Dudhia J, Chen SH (2004) A revised approach to ice microphysical processes for the bulk parameterization of clouds and precipitation. *Mon Weather Rev* 132:103–120
- Hong S, Noh Y, Dudhia J (2006) A new vertical diffusion package with an explicit treatment of entrainment processes. *Mon Weather Rev* 134:2318–2341. doi:10.1175/MWR3199.1
- Hong SY, Sunny Lim KS, Kim JH, Jade Lim JO, Dudhia J (2009) Sensitivity study of cloud-resolving convective simulations with WRF using two bulk microphysical parameterizations: ice-phase microphysics versus sedimentation effects. *J Appl Meteorol Clim* 48:61–76
- Hu Xiao-Ming, John W, Nielsen-Gammon Zhang F (2010) Evaluation of three planetary boundary layer schemes in the WRF model. *J Appl Meteorol Clim* 49:1831–1844
- Hubbert JC, Dixon M, Ellis SM, Meymaris G (2009) Weather radar ground clutter. Part I: identification, modeling, and simulation. *J Atmos Oceanic Technol* 26:1165–1180
- Janjić ZI (1994) The step-mountain Eta coordinate model: further developments of the convection, viscous sublayer, and turbulence closure schemes. *Mon Weather Rev* 122:927–945
- Jankov I, Gallus WA Jr, Segal M, Shaw B, Koch SE (2005) The impact of different WRF model physical parameterizations and their interactions on warm season MCS rainfall. *Weather Forecast* 20:1048–1060
- Kain JS (2004) The Kain–Fritsch convective parameterization: an update. *J App Meteorol* 43:170–181
- Kain J, Fritsch M (1993) Convective parameterization for mesoscale models: The Kain–Fritsch scheme. In: Eannual KA, Raymond DJ (eds) *The Representation of Cumulus Convection in Numerical Models*, Meteorological monographs, chap 16. American Meteorological Society, Boston, pp 165–170
- Kain JS, Baldwin ME, Weiss SJ (2003) Parameterized updraft mass flux as a predictor of convective intensity. *Weather Forecast* 18:106–116
- Krieger JR, Zhang J, Atkinson DE, Shulski MD, Zhang X (2009) Sensitivity of WRF model forecasts to different physical parameterizations in the Beaufort Sea region. Preprints, Eighth Conf. on Coastal Atmospheric and Oceanic Prediction and Processes, Phoenix, AZ, Amer Meteor Soc P1.2
- Kumar RA, Dudhia J, Roy Bhowmik SK (2010) Evaluation of physics options of the Weather Research and Forecasting (WRF) Model to simulate high impact heavy rainfall events over Indian Monsoon region. *Geofizika* 27:101–125
- Lin YL, Farley RD, Orville HD (1983) Bulk Parameterization of the snow field in a cloud model. *J App Meteorol* 22:1065–1092
- Litta AJ, Mohanty UC (2008) Simulation of a severe thunderstorm event during the field experiment of STORM programme 2006, using WRF–NMM model. *Curr Sci* 95:204–215
- Madala S, Satyanarayana AN, Srinivas CV, Tyagi B (2016) Performance evaluation of PBL schemes of ARW model in simulating thermo-dynamical structure of pre-monsoon convective episodes over kharagpur using STORM Data Sets. *Pure appl Geophys* 173:1803–1827
- Madhulatha A, Rajeevan M, Venkat Ratnam M, Bhate J, Naidu CV (2013) Nowcasting severe convective activity over southeast India using ground-based microwave radiometer observations. *J Geophys Res*. doi:10.1029/2012JD018174
- Melissa AG, Mullen SL (2005) Evaluation of QPF from a WRF ensemble system during the southwest monsoon. In: 6th WRF/15th MM5 users' workshop, June (pp. 27–30)
- Mellor GL, Yamada T (1982) Development of a turbulence closure model for geophysical fluid problems. *Rev Geophys Space Phys* 20:851–875
- Mlawer EJ, Taubman SJ, Brown PD, Iacono MJ, Clough SA (1997) Radiative transfer for inhomogeneous atmosphere: RRTM, a validated correlated-k model for the longwave. *J Geophys Res* 102:16663–16682
- Mohan M, Bhati S (2011) Analysis of WRF model performance over subtropical region of Delhi. *Adv Meteorol, India*. doi:10.1155/2011/621235
- Mohan TS, Rao TN (2012) Variability of the thermal structure of the atmosphere during wet and dry spells over southeast India. *Q J Roy Meteor Soc* 138:1839–1851
- Morrison H, Milbrandt J (2011) Comparison of two-moment bulk microphysics schemes in idealized supercell thunderstorm simulations. *Mon Weather Rev* 139:1103–1130
- Morrison H, Thompson G, Tatarskii V (2009) Impact of cloud microphysics on the development of trailing stratiform precipitation in a simulated squall line: comparison of one- and two-moment schemes. *Mon Weather Rev* 137:991–1007
- Mukhopadhyay P, Taraphdar S, Goswami BN (2011) Influence of moist processes on track and intensity forecast of cyclones over the north Indian Ocean. *Geophys Res* 116:D05116. doi:10.1029/2010JD014700
- Nakanishi M, Niino H (2004) An improved Mellor–Yamada level-3 model with condensation physics: its design and verification. *Bound-Lay Meteorol* 112:1–31
- Okamoto K, Iguchi T, Takahashi N, Iwanami K, Ushio T (2005) The Global Satellite Mapping of Precipitation (GSMaP) project. In: 25th IGARSS Proceeding, pp 3414–3416
- Otkin J, Huang HL, Seifert A (2006) A comparison of microphysical schemes in the WRF model during a severe weather event. In: Papers delivered at 7th WRF Users' Workshop, Boulder, CO, USA, pp. 19–22
- Pattanayak S, Mohanty UC (2008) A comparative study on performance of MM5 and WRF models in simulation of tropical cyclones over Indian seas. *Curr Sci* 95:923–936
- Pennelly C, Reuter G, Flesch T (2014) Verification of the WRF model for simulating heavy precipitation in Alberta. *Atmos Res* 135–136:172–192

- Pleim JE (2007) A combined local and nonlocal closure model for the atmospheric boundary layer. Part II: application and evaluation in a mesoscale meteorological model. *J Appl Meteor Climatol* 46:1396–1409
- Pleim JE, Chang JS (1992) A non-local closure model for vertical mixing in the convective boundary layer. *Atmos Environ* 26A:965–981
- Rajeevan M, Kesarkar A, Thampi SB, Rao TN, Radhakrishna B, Rajasekhar M (2010) Sensitivity of WRF cloud microphysics to simulations of a severe thunderstorm event over south-east India. *Ann Geophys* 28:603–619
- Rama Rao YV, Hatwar HR, Salah AK, Sudhakar Y (2007) An experiment using the high resolution Eta and WRF models to forecast heavy precipitation over India. *Pure Appl Geophys* 164:1593–1615
- Rao DVB, Prasad DH (2007) Sensitivity of tropical cyclone intensification to boundary layer and convective processes. *Nat Hazards* 41:429–445
- Ruiz Juan J, Celeste S, Julia NP (2010) WRF Model sensitivity to choice of parameterization over South America: validation against Surface Variables. *Mon Weather Rev* 138:3342–3355
- Rutledge SA, Hobbs PV (1984) The mesoscale and microscale structure and organization of clouds and precipitation in midlatitude cyclones. XII: a diagnostic modeling study of precipitation development in narrow cold-frontal rainbands. *J Atmos Sci* 41:2949–2972
- Shin HH, Hong SY (2011) Intercomparison of planetary boundary-layer parametrizations in the WRF model for a single day from CASES-99. *Bound-Layer Meteorol* 139:261–281
- Skamarock W, Klemp JB, Dudhia J, Gill D, Barker D, Duda M, Huang X, Wang, Powers J (2008) A description of the advanced research WRF version 3. NCAR Technical Note, NCAR/TN\u20132013475+STR, p 123
- Stoelinga MT, Woods CP, Locatelli JD, Hobbs PV (2005) On the representation of snow in bulk microphysical parameterization schemes. Preprints, Joint WRF/MM5 Users' Workshop, Boulder, Colorado, June 2005. NCAR Mesoscale and Microscale Meteorology Division
- Stull RB (1988) An introduction to boundary layer meteorology. Kluwer Academic Publishers, Dordrecht
- Stull RB, Driedonks AGM (1987) Applications of the transient turbulence parameterization to atmospheric boundary-layer simulations. *Bound-Lay Meteorol* 40:209–239
- Thompson G, Rasmussen RM, Manning K (2004) Explicit forecasts of winter precipitation using an improved bulk microphysics scheme. Part I: description and sensitivity analysis. *Mon Weather Rev* 132:519–542
- Thompson G, Field PR, Rasmussen RM, Hall WD (2008) Explicit forecasts of winter precipitation using an improved bulk microphysics scheme. Part II: implementation of a new snow parameterization. *Mon Weather Rev* 136:5095–5115
- Vaidya SS, Kulkarni JR (2007) Simulation of heavy precipitation over Santacruz, Mumbai on 26 July 2005, using mesoscale model. *Meteorol Atmos Phys* 98:55–66
- Wang W, Seaman LN (1996) A comparison study of convective parameterization schemes in a Mesoscale model. *Mon Weather Rev* 125:252–278
- Weverberg VK, Vogelmann MA, Lin W, Luke PE, Cialella A, Minnis P, Khaiyer M, Boer ER, Jensen PM (2012) The role of cloud microphysics parameterization in the simulation of mesoscale convective system clouds and precipitation in the tropical western pacific. *J Atmos Sci* 70:1104–1128
- Wisse JSP, de Arellano JVG (2004) Analysis of the role of the planetary boundary layer schemes during a severe convective storm. *Ann Geophys* 22:1861–1874
- Wu D, Dong X, Xi B, Feng Z, Kennedy A, Mullendore G, Gilmore M, Tao WK (2013) Impacts of microphysical scheme on convective and stratiform characteristics in two high precipitation squall line events. *J Geophys Res Atmos* 118:11119–11135 doi:[10.1002/jgrd.50798](https://doi.org/10.1002/jgrd.50798)